Doping of III–V Arsenide and Phosphide Wurtzite Semiconductors

Giacomo Giorgi, Michele Amato, Stefano Ossicini, Xavier Cartoixà, Enric Canadell, Riccardo Rurali

Doping of III-V arsenide and phosphide wurtzite semiconductors

Giacomo Giorgi,[†,‡,@] Michele Amato,[¶,@] Stefano Ossicini,[§,‖] Xavier Cartoixà,[⊥] Enric Canadell,[*,#] and Riccardo Rurali[*,#]

Department of Civil and Environmental Engineering, University of Perugia (DICA), via G. Duranti, 93, 06125 Perugia, Italy, CNR-SCITEC, 06123 Perugia, Italy, Université Paris-Saclay, CNRS, Laboratoire de Physique des Solides, 91405, Orsay, France , "Centro S^3", CNR-Istituto di Nanoscienze, via Campi 213/A, 41125 Modena, Italy, Dipartimento di Scienze e Metodi dell'Ingegneria, Centro Interdipartimentale En&Tech, Universitá di Modena e Reggio Emilia, via Amendola 2 Pad. Morselli, I-42100 Reggio Emilia, Italy, Departament d'Enginyeria Electrònica, Universitat Autònoma de Barcelona, 08193 Bellaterra, Barcelona, Spain , and Institut de Ciència de Materials de Barcelona, ICMAB–CSIC, Campus UAB, 08193 Bellaterra, Spain

E-mail: canadell@icmab.es; rrurali@icmab.es

Abstract

The formation energies of *n*- and *p*-type dopants in III-V arsenide and phosphide semiconductors (GaAs, GaP, and InP) are calculated within a first-principles total energy approach. Our

[*]To whom correspondence should be addressed
[†]University of Perugia
[‡]CNR-SCITEC
[¶]Université Paris-Sud
[§]"Centro S^3", CNR-Istituto di Nanoscienze
[‖]Dipartimento di Scienze e Metodi dell'Ingegneria, Centro Interdipartimentale En&Tech
[⊥]Universitat Autònoma de Barcelona
[#]Institut de Ciència de Materials de Barcelona
[@]These authors contributed equally to this work

findings indicate that –for all the considered systems– both the solubility and the *shallowness* of the dopant level depends on the crystal phase of the host material (wurtzite or zincblende) and is the result of a complex equilibrium between local structural distortion and electronic charge reorganization. In particular, in the case of acceptors, we demonstrate that impurities are always more stable in the wurtzite lattice with an associated transition energy smaller with respect to the zincblende case. Roughly speaking, this means that it is easier to *p*-type dope a wurtzite crystal and the charge carrier concentration at a given temperature and doping dose is larger in the wurtzite as well. As for donors, we show that neutral chalcogen impurities have no clear preference for a specific crystal phase, while charged chalcogen impurities favor substitution in the zincblende structure with a transition energy that is smaller if compared to the wurtzite case (thus charge carriers are more easily thermally excited to the conduction band in the zincblende phase).

Keywords

Polytypism, nanowires, crystal phase engineering, wurtzite, GaAs, InP, GaP, dopants, density functional theory, formation energy

Introduction

Crystal phase engineering is an emerging field in nanoscience that consists in the design of materials with tailor-made properties by growing *ad hoc* crystal phases. The interest in this field was boosted by the enormous progresses made in recent years in the growth of semiconducting nanowires (NWs)[1,2] and, specifically, by the fact that metastable crystal phases, which in bulk can only be obtained under extreme conditions of temperature and pressure, can be stabilized at room temperature and atmospheric pressure, thanks to a tight control of growth conditions.[3] Many III-V semiconductors, such as arsenides[4–7] and phosphides,[8–11] that in bulk only exhibit the zincblende (ZB) phase, can take the wurtzite (WZ) structure when grown as NWs. Similarly, Si and Ge group-

IV semiconductors that in bulk have the 3C cubic-diamond crystal structure, can by synthesized in the 2H hexagonal-diamond (i.e. lonsdaleite) polytype.[12–15] The possibility of growing semiconductors in different crystal phases is very appealing, as it might enable novel applications.[16] For instance, ZB GaP has an indirect bandgap and thus a limited light emission efficiency, but in WZ GaP NWs, the bandgap becomes direct, resulting in a strong photoluminescence.[9] Direct-bandgap emission has also been predicted and reported in hexagonal Ge and SiGe alloys,[17,18] materials that have a notoriously poor light emission in the conventional cubic polytype adopted in the bulk. More in general, different polytypes can present different electronic[7,19–21] optical[22–26] and phononic properties.[27–31]

Perhaps, the most ambitious (and exciting) goal of crystal phase engineering is the design of complex structures by playing only (or mostly) with different polytypes of the same material. The conditions that favor the formation of WZ over ZB segments in III-V NWs are well understood[32–34] and can be dynamically tuned during the growth. Therefore, not only isolated *homointerfaces* between the ZB and the WZ crystal phase of a same material can be obtained,[22,35–37] but also periodic superlattice structures. In these crystal phase superlattices, different polytypes of the same material –rather than different materials, like in conventional superlattices– are arranged periodically, building a metamaterial with its own unique properties, which can be tuned by controlling the number of periods and their thickness.[38–41] These crystal phase interfaces present some advantages over the most common heterojunctions between two different materials: (i) they have a very small lattice mismatch and (ii) they have no chemical intermixing. As a result, they are atomically flat and virtually defect-free, what makes them ideal candidates to design materials with tailored electronic[38,42,43] and phononic properties.[44,45] Similar effects have also been reported in the less common crystal phase core-multishell NWs.[46,47]

The vast majority of applications that can be envisaged in this context relies on impurity doping, which is the primary approach to tune the electrical conductivity of semiconductors. Indeed, the design of electronic devices is based on the juxtaposition of regions with different doping features, e.g. in a *pn* junction, in a bipolar transistor or in a field-effect transistor. Therefore, a detailed understanding of doping in different crystal phases is necessary, both from the viewpoint of the fundamental understanding of the underlying physical mechanisms and for the operation of a multitude of applications. Given a material, is it equally easy to dope it in the ZB and in the WZ phase? Is the dopant activation energy the same or does it differ in different polytypes? The answers to these questions tell us how the solubility and the charge carrier concentration depend on the crystal phase and have thus far reaching consequences for the design and the optimization of any device.

In this paper we study by means of first-principles electronic structure calculations the doping of GaAs, GaP, and InP in the ZB and in the WZ crystal phase, considering a few common donor and acceptor impurities and an amphoteric impurity (Si in GaAs), whose doping type –donor or acceptor– depends on the sublattice where the substitution takes place. We consider both the neutral and the singly-charged impurity, thus allowing to estimate the transition energy, i.e. the *shallowness* of the dopant electron state, which determines the concentration of extrinsic charge carriers that are excited in the conduction or valence band for a certain doping dose and at a given temperature, and thus the electrical conductivity. We carry our calculations in bulk systems, as a reasonable approximation of NWs with diameters of several tens of nm and where quantum confinement effects are negligible, which are commonly used in emergent electronic devices. We observe, nonetheless, that previous results obtained for Si showed that ultrathin NWs (diameters of ~ 2 nm) and bulk systems qualitatively exhibit the same behavior regarding the difference between the cubic and hexagonal crystal phase.[43]

Computational methods

Electronic structure calculations

We perform density-functional theory (DFT) calculations with the VASP code[48] with the local density approximation (LDA) for the exchange-correlation energy functional. We used a plane wave cutoff ranging from 255.2 to 400 eV, depending on the atomic species involved, with the projector augmented-wave method,[49,50] including semicore d electrons for Ga and In. At first we optimized the lattice parameters of the ZB and WZ primitive cells, sampling the Brillouin zone with a $10 \times 10 \times 10$ and a $10 \times 10 \times 6$ grid of **k**-points, respectively. Our results are shown in Table 1. Substitutional impurities at both the group-III and group-V sublattice were studied in $5 \times 5 \times 5$ and $5 \times 5 \times 3$ supercells of the 2- and 4-atom ZB and WZ primitive cell, with a $2 \times 2 \times 2$ grid of **k**-points. The geometry of the doped supercells was optimized with a quasi-Newton algorithm until all the forces on the atoms were lower than 0.01 eV/Å. This computational setup proved to be accurate enough to give converged values of the formation energy, as shown in previous theoretical studies.[51–54]

We also performed density-functional perturbation theory (DFPT) to compute the macroscopic dielectric tensor, explicitly accounting for local field effects, which is needed for the charge correction scheme described below. We used the optimized lattice vectors and atomic positions obtained at the single-particle DFT level. The computational parameters are the same of the DFT calculations, but we found that greatly increased **k**-points meshes are needed to obtain converged results. We used a $36 \times 36 \times 36$ and $36 \times 36 \times 22$ grid for the ZB and the WZ polytypes, respectively. The results are summarized in Table 1.

On top of the previously optimized primitive cells we performed *single-shot* G_0W_0 calculations, where quasi-particle energies are calculated from a single GW iteration i.e., using the screened potential (W) as obtained from the DFT (LDA) step. To improve the quality of the results, a large number of real frequency points (200) has been employed for Hilbert transform of W and self-energy, Σ. Similarly, a very large number of empty bands (~ 200) has been included in the calculations to ensure convergence of the results.

Handling of computational cells with net charge

Plane-wave DFT codes, but also localized-basis-set codes with a Poisson solver based on reciprocal space, assume that the system extends *ad infinitum* with the periodicity set at the input for the computational cell. For charge neutral systems, this use of periodic boundary conditions (PBCs) is of course well justified in bulk 3D systems, and in lower dimensionalities it poses no special difficulties, provided that a thick enough vacuum buffer is added to prevent interaction between the (spurious) system replicas.

The situation is, however, different when addressing systems with isolated net charges, such as the case with an ionized dopant of interest to us here. The long-range Coulomb interaction between the PBC-induced charge replicas will introduce a spurious contribution to the total energy that must be corrected for. Several correction schemes have been proposed[55–58] (see also Ref. 59 and references therein), often involving the computation of the Madelung energy for some geometric arrangement of point charges in a compensating background.[60,61] In this work we use a variant of the Makov-Payne scheme[56] that some of us extended to the case of arbitrary shape of the computational cell and tensor value of the dielectric constant,[62] which is necessary for the hexagonal cells in the WZ case. This type of correction was shown to accelerate convergence in the case of nanowires,[63] and thus it is also expected to do it here.

The elements of the dielectric tensor that we have used for our Madelung correction have been obtained from a DFPT calculation as detailed above. We do not consider it necessary to correct these dielectric tensor entries by their experimental counterparts, given that the interaction between the point charge replicas will be screened according our used theory level, *i. e.* LDA.

Formation energy

The formation energy is the central quantity in defect analysis and it tells us how likely it is to observe a defect in a crystal matrix,[59] either in the case of intrinsic imperfections of the crystal lattice or –the case addressed here– when it comes to an impurity added on purpose to alter in a controlled way the property of a material. The knowledge of the formation energy of a defect delivers some important information concerning the impurity equilibrium concentrations,[64–66] the solubilities,[67,68] or the diffusivities.[69,70] Additionally, by comparing the formation energy of a neutral and a singly-charged defect one can obtain the transition energy, a quantity of paramount importance in semiconductor physics that tells us which is the energy needed to thermally excite carriers from the dopant state to the conduction or valence band. The formation energy, as introduced by Zhang and Northrup,[64] is written as follows:

$$E_{\text{form}} = E_{\text{tot}}^{D} - \sum_{i} n_i \mu_i + q(\mu_e + E_V) \tag{1}$$

where E_{tot}^{D} is the total energy of the system including the defect, the sum runs over all the chemical species present and n_i and μ_i are the number of atoms and chemical potential of species i; q is the charge state of the defect, μ_e is the chemical potential of the electron, which is referred to E_V, the highest occupied eigenvalues of the pristine system. Therefore, μ_e varies from 0 –at the top of the valence band– to E_{gap} –at the bottom of the conduction band–, thus spanning the whole range of doping conditions.

In the case of a compound semiconductor like the ones studied in this work, Eq. 1 is conveniently reformulated as:[65]

$$\begin{aligned} E_{\text{form}} &= E_{D}^{\text{tot}} - \frac{1}{2}(n_{\text{Ga}} + n_{\text{As}})\mu_{\text{GaAs}}^{\text{bulk}} - \frac{1}{2}(n_{\text{Ga}} - n_{\text{As}})(\mu_{\text{Ga}}{}^{\text{bulk}} - \mu_{\text{As}}{}^{\text{bulk}} + \Delta\mu) + \\ & \quad q\,(\mu_e + E_V) - n_X \mu_X \end{aligned} \tag{2}$$

which, for simplicity, we have written in the case of GaAs with a generic impurity X. The chemical potentials $\mu_{\text{Ga}}^{\text{bulk}}$, $\mu_{\text{As}}^{\text{bulk}}$, and $\mu_{\text{GaAs}}^{\text{bulk}}$ refer to the bulk compound of Ga, As, and GaAs. We computed $\mu_{\text{Ga}}^{\text{bulk}}$ and $\mu_{\text{As}}^{\text{bulk}}$ as the energy per atom of Ga and As in the orthorhombic and trigonal phase, respectively; for $\mu_{\text{GaAs}}^{\text{bulk}}$ we considered the ZB or the WZ crystal phase, depending on the case being addressed. Notice that μ_{Ga} and μ_{As} are the chemical potential of Ga and As *in* GaAs and that computing their value is not straightforward. However, one can observe that the chemical potential of bulk GaAs is $\mu_{\text{GaAs}}^{\text{bulk}} = \mu_{\text{Ga}}^{\text{bulk}} + \mu_{\text{As}}^{\text{bulk}} - \Delta H_f$, where ΔH_f is the heat of formation of GaAs. Now E_{form} is a function of the bulk chemical potential of Ga and As and of the parameter $\Delta\mu$ that accounts for the difference between the chemical potentials of Ga and As in GaAs and in their respective bulk state. The reformulation of E_{form} in Eq. 2 has the advantage of expressing it in terms of well defined quantities (the bulk chemical potentials) and of the parameter

$$\Delta\mu = (\mu_{\mathrm{Ga}} - \mu_{\mathrm{As}}) - (\mu_{\mathrm{Ga}}{}^{\mathrm{bulk}} - \mu_{\mathrm{As}}{}^{\mathrm{bulk}}) \tag{3}$$

which accounts for the macroscopic stoichiometry conditions of the material. $\Delta\mu$ can vary between $-\Delta H_f$, limit that corresponds to the As-rich condition, and ΔH_f, for the Ga-rich material, condition fixed by the inequalities $\mu_{\mathrm{Ga}} \leq \mu_{\mathrm{Ga}}{}^{\mathrm{bulk}}$ and $\mu_{\mathrm{As}} \leq \mu_{\mathrm{As}}{}^{\mathrm{bulk}}$. This formalism is also applied to the case of GaP and InP, where we considered the cubic phase for bulk P and the trigonal phase for bulk In to define $\mu_{\mathrm{P}}^{\mathrm{bulk}}$ and $\mu_{\mathrm{In}}^{\mathrm{bulk}}$.

In the case of the chemical potential of the dopant, μ_X ($X =$ Si, C, Zn, S, Te) we have taken the energy of the isolated atom, assuming that the impurity is incorporated into the crystal from the gas phase. This choice, though sound, is an approximation, because the chemical reservoir where the impurity comes from is not necessarily the one of a monoatomic gas. A different choice would result in a different value of the formation energy (see e.g. Ref. 71 for a discussion of the case of H in SiC). Notice, however, that whenever we compare the formation energy of a given impurity in the ZB or in the WZ crystal phase, μ_X cancels out and thus the conclusions do not depend on its exact value, as already shown in Refs. 53,54. The same happens when comparing the formation energy of a dopant in the neutral and singly-charged state, which determines the transition energy (neither the transition energy depends on μ_X).

Results and Discussion

Stability and bandgap of the pristine bulk systems

Before discussing impurity doping it is instructive to revise the theory that explains why a given semiconductor adopts one crystal structure or the other, as it will then be important to understand the stability of dopants as well.

The simplest way to understand the difference between the ZB and the WZ crystal phases is by looking at the stacking sequence along the [111] cubic axis, which is equivalent to the [0001] axis of the wurtzite. As it is easy to see in Figure 1(a)-(b), in the ZB crystal structure the III-V bilayers are stacked one on top of the other according to an ABCABC stacking motif, while in the WZ one they follow an ABABAB stacking sequence. When III-arsenides or a III-phosphides form, the starting point is always the AB stacking as the sequence of two bilayers of the same type, e.g. AA, is energetically unfavorable. When the next layer grows it can take the A or the C position and thus the ZB or the WZ symmetry. In other words, the two polytype structures differ only in the eclipsed (WZ) or staggered (ZB) dihedral conformation that in turn affects the 1,4 atomic interactions (see in Figure 1(c)-(d)). Under such conditions the preference for one of the two crystal phases is the result of a competition between covalent and ionic contributions.[72,73] For compounds following the octet rule, $A^{N}B^{8\text{-}N}$, the WZ structure is favored when the ionic component is strong. The limiting case is constituted by group-IV semiconductors, i.e. Si, Ge, and diamond, where the bond is fully covalent and that accordingly adopt the cubic structure. Then, in III-V semiconductors, the larger is the ionic contribution, the less the ZB phase will be favored over the WZ, until the latter becomes the ground state as in GaN.

Our results agree well with this picture, as we found that the preference for the ZB structure according to our calculations is 21.9 meV for GaAs, 17.4 meV for GaP, and 10.6 meV for InP per unit formula (f.u.), which follows a prediction based on the electronegativity differences between anion and cation according to the Pauling scale, a crude measure of the ionicity of the bond: 0.37 for GaAs, 0.38 for GaP, and 0.41 in InP. Therefore, the larger the electronegativity difference, the more ionic is the bond and the less favored is the ZB crystal phase. A more refined definition of the ionicity of a bond is the so-called atomic asymmetry parameter (AAS) between a pair of atoms,[74,75] which is known to work well in crystals of the $A^{N}B^{8\text{-}N}$ type. The AAS values for GaAs, GaP, and InP are 0.316, 0.371 and 0.506, which are also in good agreement with the above mentioned energy preferences. Other criteria to estimate the ionic character of chemical bond are of course possible, see e.g. the ionicity scale based on the centers of maximally localized Wannier functions of Abu-Farsakh and Qteish.[76]

One of the reasons of interest in crystal phase engineering is the tunability of the electronic properties. Therefore, another issue that we addressed and briefly discuss before moving to the case of extrinsic doping is the dependence of the electronic bandgap on the crystal phase. As it is well known, DFT in its local and semilocal approximation of the exchange-correlation energy severely underestimates the bandgap. Therefore, we have performed quasiparticle G_0W_0 calculations that allow bypassing this limitation. The results are reported in Table 1.

The electronic properties of bulk ZB GaAs have been investigated from first-principles since decades in view of the microelectronics oriented applications of the material[77–80] and theoretical assessing the bandgap of GaAs main polymorphs remains controversial, as a definitive conclusion is still missing (see Ref. 16 for a detailed discussion). Furthermore, while on one side there is large availability of experimental data about ZB GaAs (see e.g.[81,82]), the scarcity of experimental data about WZ GaAs samples, mostly derived by NW structures, makes the comparison with experimental data for this polymorph a quite cumbersome task due to the expected overestimation of the gap because of quantum confinement effects. Indeed, there are experimental reports for the band gap of WZ-GaAs NWs to be either larger or smaller than the one of ZB-GaAs NWs by few tens of meV.[16]

A good description and comparison between DFT and GW calculated electronic properties of the two polymorphs of GaAs has been provided by Zanolli *et al.*:[83] their LDA calculated value for WZ GaAs is 50 meV larger than the ZB calculated one in good agreement with our findings (the absolute values differ because Zanolli *et al.* used a different, custom made pseudopotential[84]) and with those of Yeh *et al.*[78] On the other hand, the GW values they obtain are 1.133 eV (ZB) and 1.351 eV (WZ), while at the quasiparticle level we found the bandgap of ZB GaAs to be larger than WZ GaAs (see Table 1).

A similar problem can be encountered in the case InP and GaP. Since the WZ bulk phase of these compounds is not stable under normal conditions, all the experimental data concerning its band gap are derived from indirect measurements on NWs (in which instead the WZ phase can be stabilized). Theoretical and experimental literature addressing this issue is less extensive if compared to GaAs. The band gap of WZ InP has been experimentally reported to be slightly larger than that of ZB InP (see for instance Refs.[85,86]), in agreement with our results (see Table 1) and other theoretical calculations.[87] On the other hand a limited number experiments has been performed to investigate the band gap of WZ GaP,[9,26] which is expected to be around 2.19 eV. This value is not far from what we calculated (2.28 eV) and other *ab initio* quasiparticle calculations.[88]

Impurity doping: stability and transition energies

General considerations

Band theory of semiconductors relies on a perfect duality between *n*- and *p*-type doping, where electrons and holes are thermally excited from the impurity state to the conduction and valence band. Microscopically, however, this duality breaks down, because chemical bonds are formed by electrons only. Therefore, the case of donors, where the four bonds of a tetrahedral semiconductor can be satisfied and there is an additional, loosely bound electron, is different from the case of acceptors, where the substitutional impurity only has three electrons to form bonds.

In the ZB phase all atoms occupy the center of a perfect tetrahedron with all four first neighbors distances equal (T_d symmetry). This local symmetry is maintained in the case of doping with deformations consisting in the sole uniform contraction or expansion of the bond length. In the WZ phase, each atom has three equidistant first neighbors, while the fourth neighbor, along the c direction, is usually more far apart (C_{3v} symmetry). The WZ structure has thus more structural freedom to adjust to perturbations induced by impurities, because the variations in the bonding can be tuned by the fact that there are two different types of bonds. Therefore, when an acceptor is introduced in the lattice, it will try to form three bonds, something that is favored in the WZ structure where three of the bonds can become stronger and one weaker, the final outcome being a stabilization of the lattice. This does not happen in the ZB lattice. Thus introducing electron deficiency in the pristine III-V solids provides a bias for the WZ structure.[53]

Another way of tuning the WZ-ZB stability is by altering the ionic component of the bonding. In III-V solids the bond is always partly ionic and one partner is electron-rich, whereas the other is electron-poor. Adding electrons or holes has different effects: adding electrons increases the electronic asymmetry and thus the ionic contribution, whereas adding holes decreases the electronic asymmetry and thus the ionic contribution. Accordingly to the discussion of the previous section, an increased ionicity favors the WZ lattice, while more covalent bonds favor the ZB. Therefore, adding (removing) electrons is expected to stabilize the WZ (ZB) crystal phase.

Acceptors

We now move to the discussion of the main results of our study and start with impurities that provide *p*-type doping. We computed the formation energies of five different systems doped with an acceptor: C_{As}@GaAs, Si_{As}@GaAs, Zn_{Ga}@GaAs, Zn_{Ga}@GaP, Zn_{In}@InP, where the notation C_{As}@GaAs stands for a C substituting an As atom in a GaAs lattice (and likewise for the other cases). In all the cases we considered the neutral charge state and the -1 charge state, which is expected to be the more stable charge state when the Fermi level lies above the dopant level. These are all textbook cases of acceptors, where an atom of the lattice is substituted by an impurity from the group of the periodic table immediately at its left. Impurities from group-IV can, in principle, be both donors and acceptors, depending on the sublattice chosen for the substitution.[89] This is the case of Si@GaAs, which acts as an acceptor when it substitutes an As and as a donor when it substitutes a Ga. C could behave similarly, but substitution at the As sublattice is much more stable than substitution at the Ga sublattice (we found a difference of 0.27 and 0.37 eV in ZB and WZ GaAs, respectively), so that the latter in practice never occurs. We recall that we carry out our calculations in bulk systems, as an approximation of realistic, large diameter NWs. For a study of extrinsic defects in GaAs NWs the interested reader can see e.g. the works of Galicka *et al.*[90] and Diao *et al.*;[91] intrinsic defects in GaAs and their relation with polytypism have been explored by Du *et al.*[92]

The results of the formation energy as a function of the chemical potential of the electron for GaAs are shown in Figure 2. As it can be seen, all the three acceptors have some features in common: (i) the neutral impurity is always more stable in the WZ lattice, for all values of μ_e (see dashed lines in Figure 2); (ii) the increased stability is similar in all the cases; (iii) the transition energy is (slightly) smaller in the WZ and the impurity state is *shallower* (see the zoomed view for Si_{As}@GaAs). Simply put, it is easier to *p*-type dope GaAs in the WZ phase and these dopants will be easier to activate.

Following the arguments given above, we now attempt to rationalize the observed behavior. A very important factor to consider in understanding the role of the impurity is the mismatch between the impurity and the host lattice. The four Ga-As bond lengths in pristine WZ GaAs are 2.422 (x3) and 2.433 Å. Let us consider the case of Si_{As}@GaAs (the full list of bond lengths is given in the Supporting Information). The Si-As bond lengths around the impurity are 2.348 (x3) and 2.353 Å, i.e. they are all shorter because Si is smaller than As. The four distances associated with the four nearest-neighbor Ga atoms are 2.440-2.430 (x3) and 2.348-2.353 Å. This means that the structural perturbation of the impurity is almost limited to the second coordination sphere of the impurity. However, more important to notice is the fact that the three bonds for every nearest-neighbor of the impurity connecting with the rest of the GaAs lattice are longer than in the pristine. In other words, the stabilizing effect due to the four bonds of the Si impurity are at least partially compensated by the destabilization of the twelve Ga-As bonds of the second coordination sphere. Of course, this effect occurs even more intensely for the case of C_{As}@GaAs. A different situation occurs for Zn_{Ga}@GaAs. In that case the Zn-As distances are 2.395 (x3) and 2.397 Å, which are shorter than the initial ones, but not as much as for Si. However, now the distances connecting the four nearest-neighbors with the rest of the GaAs lattice are all around 2.390-2.400 Å, i.e. they are all shorter than the initial ones. Clearly, the better match between the impurity and the host lattice allows a weaker but better balanced distortion of the lattice which avoids the above mentioned destabilization of twelve bonds and transforms it into stabilization.

For all neutral acceptor impurities studied (Table 2) we find that, whatever the mismatch is, the WZ structure is clearly preferred. This is the consequence of two features, both already anticipated in the discussion of the previous section: (i) acceptor impurities generate electron deficiency in the already electron deficient sites of the lattice, and (ii) as far as the impurity is smaller or similar in size to the original host atom, the induced structural perturbation is more easily accommodated within the WZ lattice, because of the larger structural freedom degrees allowing a 3+1 type coordination. As shown in Table 2 this preference is even increased for the charged impurities. Thus, the transition energies for acceptor impurities are always smaller (i.e. the impurity level is closer to the valence band, $\Delta E(0/-)$ in Table 2) in the WZ structure. If we consider impurities in the GaAs lattice, it is clear that the increase in the preference when the impurity is charged is an almost constant value (the only exception is singly-charged Si that does not favor any crystal phase). By analyzing the Bader charges before and after the charging we could conclude that there is barely any change at the impurity and four nearest-neighbors sites, thus suggesting that the hole resulting from the acceptor impurity must be very delocalized in the lattice. Since adding an electron increases the charge asymmetry, the WZ should be further stabilized over the ZB because of the charging although the effect is only modest for acceptor impurities. Consequently, our calculations suggest that smaller transition energies will be associated with larger stabilizations of the WZ structure for the neutral impurity.

All these considerations are straightforwardly extended to the case of Zn_{Ga}@GaP and Zn_{In}@InP, whose formation energies are shown in Figure 3 and 4, and thus confirm the generality of the trends discussed.

Donors

We considered four different systems doped with a donor: Si_{Ga}@GaAs, S_P@GaP, Te_P@GaP, and Te_P@InP. In all these cases an atom of the lattice is substituted by an impurity from the group of the periodic table immediately at its right. We studied each impurity in the neutral and $+1$ charge state, which is expected to be the more stable charge state when the Fermi level lies below the dopant level. As mentioned above, Si is an amphoteric dopant, so while Si_{As}@GaAs was an acceptor, here we study Si_{Ga}@GaAs that acts as a donor.

The results of the formation energy as a function of the chemical potential of the electron for the three compounds investigated are shown in Figures 2-4. Also in this case it is possible to highlight some common features: (i) neutral chalcogen impurities, S and Te, show no clear preference for the ZB or the WZ crystal phase; (ii) charged chalcogen impurities favors substitution in the ZB structure; (iii) the transition energy is smaller in the ZB, i.e. the impurity state is *shallower* (see the zoomed view of Si_{Ga}@GaAs, Te_P@GaP, and Te_P@InP, in the side panels). Therefore, at variance with the case of acceptors, donor impurities are more easily activated in the ZB crystal phase, while their solubility is larger in ZB structures when the impurities are in the $+1$ charge state. We note that occasionally the transition energy falls within the conduction band, this being a known shortcoming of using LDA to account for the exchange-correlation energy and thus of the underestimation of the bandgap. We have indeed computed much more accurate bandgaps from G_0W_0 calculations, but treating the doped supercells at the same level of the theory is beyond the current computational capabilities and, obviously, single-particle and many-body results cannot be mixed together. Therefore, the conclusions directly related to transition energies obtained from DFT-LDA calculations can only be taken to be semiquantitative[59] and approaches that suggest to ignore the calculated band edges and reference charge transition levels to marker levels[93] or to the average electrostatic potential[94–96] have been proposed. We recall once again, however, that our main goal is understanding the difference between doping with a certain impurity the ZB and the WZ crystal phase of a given semiconductor, and not to quantitatively estimate the transition energies. Hence, we argue that all the conclusions based on such comparisons are robust and the physical insight they provide is reliable.

The donors that we studied belong to two different categories. When P is substituted by S or Te neutral impurities, a structural perturbation different from those discussed above takes place. Both atoms are strongly electronegative and although they act as donors toward the lattice by generating an extra electron, they also gain electron density. For instance, the calculated Bader charges for S_P@GaP and Te_P@GaP are 6.85 and 6.38 e^-, respectively, in the WZ structure and 6.83 and 6.42^- in the ZB structure (for comparison, the Bader charge of P in the pristine GaP lattice amounts to 5.70 e^- in the ZB and 5.72 e^- in the WZ; remind that, do to the inclusion of 3*d* electrons in the valence of Ga atom, the total charge for each Ga-P pair is 18 e^-). In fact, this electronic gain mostly originates from the polarization of the bonds between the very electronegative chalcogen atom and the weakly electronegative Ga atom. The important structural observation is that, in contrast with acceptors, the bonds between the chalcogen and the four nearest neighbors become clearly longer than in the pristine crystal. For instance, the Ga-P bonds in WZ GaP are 2.327 (x3) and 2.338 Å. The X-Ga (X = S, Te) bond lengths around the impurity in X_P@GaP are as long as, 2.407 (x3) and 2.413 Å for X = S, and 2.610 (x3) and 2.617 Å for X = Te. The anionic chalcogen atoms, with their high electron density, strongly push the four nearest-neighbor atoms compressing the lattice around the second coordination sphere of the impurity. Under such circumstances the additional structural degree of freedom of the WZ structure becomes considerably less effective and the very isotropic nature of the ZB structure becomes comparable or even slightly preferred. Only for the more expanded lattice of InP the WZ structure is again slightly favored (see Table 3).

In contrast, because of the structural mismatch, Si_{Ga}@GaAs behaves in the same way described above for the case where Si was acting as an acceptor; the only difference is that the short distances with the four nearest neighbors are now a bit longer (i.e. 2.372 (x3) and 2.382 Å for Si_{Ga} compared with 2.348 (x3) and 2.353 Å for Si_{As} in GaAs WZ). Thus, according to our calculations, Si in GaAs has a preference for WZ irrespective of acting as a donor or an acceptor. In fact the calculated energy differences are comparable (187 meV/f.u. for Si_{As} and 152 meV/f.u. for Si_{Ga}). This result emphasizes the key role of the mismatch in enforcing the WZ-ZB preference.

Notice that among the different impurities studied, charging the impurity always favors the ZB structure even when the impurity is smaller than the host atom replaced (Table 3). This contribution is relatively large and finally determines the preference of all donor impurities studied for the ZB structure. We believe the origin of this result is that, as noted above, removing the electron provided by the neutral impurity decreases the ionicity of the lattice and consequently the ZB structure is favored. According to our calculations, for donors compressing the lattice around the impurity the shallowness will increase with the size of the impurity and/or decreasing the cell constants of the pristine lattice.

As a final remark, we observe that our computed transition energies, indicating that donor states are shallower in the ZB crystal phase, agree well with the predictions of the hydrogenic model of substitutional impurities within the Effective Mass Theory (EMT). Within this simple model, the substitutional impurity form four bonds with the nearest-neighbors, with negligible relaxation effects and charge transfer, leaving one unpaired electron whose energy is approximately given by

$$E_n \sim -\mathrm{Ry}\frac{m^*}{\varepsilon^2 n^2} \tag{4}$$

where m^* is the effective mass in units of the electron mass, n the main quantum number, ε is the (relative) static dielectric constant, and Ry is the Rydberg constant. This is the quantum-mechanical solution of the hydrogen atom except for the fact that it contains parameters of the bulk host crystal, such as m^* and ε. E_n is the energy of the unpaired electron relative to the conduction band minimum, so that large values of ε and small values of m^* both contribute to make the impurity shallower, i.e. E_n small. If we look at the computed values of the static dielectric constant collected in Table 1, we see that, for both GaAs, GaP, and InP, when going from the ZB to the WZ it decreases (with a reduction that is slightly more pronounced for the zz component of the tensor). As for the electron effective mass, it has been shown experimentally that it is heavier in the WZ than in the ZB,[36,37,97,98] a trend corroborated by our calculations. Therefore, both these effects tend to make the impurity state deeper in the WZ, in agreement with the computed transition energies. EMT also provides an estimate for the effective Bohr radius of the ground-state, which is

$$a_B \sim (\varepsilon/m^*)a_0 \tag{5}$$

where $a_0 \sim 0.577$ Å is the Bohr radius of the isolated hydrogen atom. The effective Bohr radius gives a useful indication of the distance over which the dopant wavefunction extends. This value ranges from 0.5 to 11 nm, indicating that the wavefunction can be considerably delocalized and that the donor electron loosely binds to the dopant atom. This observation agrees with the computed Bader charge of the donors that barely change when the system goes from neutral to charged, i.e. the additional charge effectively spreads all over the atoms of the supercell.

Conclusion

We have presented first-principles density-functional calculations of impurity doping in GaAs, GaP, and InP, comparing their stability and transition energies when dopants are introduced in the ZB or in the WZ. The cubic ZB crystal structure is the common crystal phase of bulk arsenides and phosphides, but doping of the WZ is becoming increasingly important, because this crystal phase can be stabilized even at room temperature and atmospheric pressure when these semiconductors are grown as NWs. Our results highlight a general trend where acceptors favor substitution in WZ crystals, where they have shallower electronic state, allowing an easier excitation of charge carriers for band transport. The situation is reversed for donors, which feature shallower impurity state and higher solubilities in the ZB. These observations are rationalized in terms of the local distortion and electronic charge reorganization upon doping. In particular we show that (i) the reduced symmetry of the WZ is better suited to accommodate the local relaxation of acceptors, which favor to a three-fold coordination; (ii) ionic bonds favor the WZ lattice, while more covalent bonds favor the ZB and that the ionic character of the bond can be increased (decreased) by adding electrons (holes). These results are important for the design and optimization of electron devices based on semiconducting nanowires in the growing field of crystal phase engineering.

Supporting Information. First-neighbor distances of the pristine crystal, of the impurity and of the four first-neighbors.

Acknowledgement

We acknowledge financial support by the Ministerio de Economía, Industria y Competitividad (MINECO) under grants FEDER-MAT2017-90024-P and PGC2018-096955-B-C44, the Severo Ochoa Centres of Excellence Program under Grant SEV-2015-0496, and the Generalitat de Catalunya under grants no. 2017 SGR 1506. We thank the Centro de Supercomputación de Galicia (CESGA) for the use of their computational resources. MA acknowledges the ANR HEXSIGE project (ANR-17-CE030-0014-01) of the French Agence Nationale de la Recherche. Part of the highperformance computing (HPC) resources for this project was granted by the Institut du developement et des ressources en informatique scientifique (IDRIS) under the allocation A0040910089 via GENCI (Grand Equipement National de Calcul Intensif). SO acknowledges support/funding from University of Modena and Reggio Emilia under project FAR2017INTERDISC GG acknowledges PRACE for awarding the access to the Marconi system based in Italy at CINECA and the Italian ISCRA program.

References

(1) Wang, N.; Cai, Y.; Zhang, R. Growth of nanowires. *Mater. Sci. Eng. R* **2008**, *60*, 1–51.

(2) Schmidt, V.; Wittemann, J. V.; Senz, S.; Gösele, U. Silicon Nanowires: A Review on Aspects of their Growth and their Electrical Properties. *Adv. Mater.* **2009**, *21*, 2681–2702.

(3) Caroff, P.; Bolinsson, J.; Johansson, J. Crystal Phases in III–V Nanowires: From Random Toward Engineered Polytypism. *IEEE Journal of Selected Topics in Quantum Electronics* **2011**, *17*, 829–846.

(4) Koguchi, M.; Kakibayashi, H.; Yazawa, M.; Hiruma, K.; Katsuyama, T. Crystal Structure Change of GaAs and InAs Whiskers from Zinc-Blende to Wurtzite Type. *Jap. J. Appl. Phys.* **1992**, *31*, 2061.

(5) Persson, A. I.; Larsson, M. W.; Stenström, S.; Ohlsson, B. J.; Samuelson, L.; Wallenberg, L. R. Solid-phase diffusion mechanism for GaAs nanowire growth. *Nature Mater.* **2004**, *3*, 677–681.

(6) Harmand, J. C.; Patriarche, G.; Péré-Laperne, N.; Mérat-Combes, M.-N.; Travers, L.; Glas, F. Analysis of vapor-liquid-solid mechanism in Au-assisted GaAs nanowire growth. *Appl. Phys. Lett.* **2005**, *87*, 203101.

(7) Funk, S.; Li, A.; Ercolani, D.; Gemmi, M.; Sorba, L.; Zardo, I. Crystal Phase Induced Bandgap Modifications in AlAs Nanowires Probed by Resonant Raman Spectroscopy. *ACS Nano* **2013**, *7*, 1400–1407.

(8) Mohan, P.; Motohisa, J.; Fukui, T. Controlled growth of highly uniform, axial/radial direction-defined, individually addressable InP nanowire arrays. *Nanotechnology* **2005**, *16*, 2903.

(9) Assali, S.; Zardo, I.; Plissard, S.; Kriegner, D.; Verheijen, M. A.; Bauer, G.; Meijerink, A.;

Belabbes, A.; Bechstedt, F.; Haverkort, J. E. M.; Bakkers, E. P. A. M. Direct Band Gap Wurtzite Gallium Phosphide Nanowires. *Nano Lett.* **2013**, *13*, 1559–1563.

(10) Vu, T. T. T.; Zehender, T.; Verheijen, M. A.; Plissard, S. R.; Immink, G. W. G.; Haverkort, J. E. M.; Bakkers, E. P. A. M. High optical quality single crystal phase wurtzite and zincblende InP nanowires. *Nanotechnology* **2013**, *24*, 115705.

(11) Lehmann, S.; Wallentin, J.; Mårtensson, E. K.; Ek, M.; Deppert, K.; Dick, K. A.; Borgström, M. T. Simultaneous Growth of Pure Wurtzite and Zinc Blende Nanowires. *Nano Lett.* **2019**, *19*, 2723–2730.

(12) Vincent, L.; Patriarche, G.; Hallais, G.; Renard, C.; Gardès, C.; Troadec, D.; Bouchier, D. Novel Heterostructured Ge Nanowires Based on Polytype Transformation. *Nano Lett.* **2014**, *14*, 4828–4836.

(13) Hauge, H. I. T.; Verheijen, M. A.; Conesa-Boj, S.; Etzelstorfer, T.; Watzinger, M.; Kriegner, D.; Zardo, I.; Fasolato, C.; Capitani, F.; Postorino, P.; Kölling, S.; Li, A.; Assali, S.; Stangl, J.; Bakkers, E. P. A. M. Hexagonal Silicon Realized. *Nano Lett.* **2015**, *15*, 5855–5860.

(14) Hauge, H. I. T.; Conesa-Boj, S.; Verheijen, M. A.; Koelling, S.; Bakkers, E. P. A. M. Single-Crystalline Hexagonal Silicon-Germanium. *Nano Lett.* **2017**, *17*, 85–90.

(15) Vincent, L.; Djomani, D.; Fakfakh, M.; Renard, C.; Belier, B.; Bouchier, D.; Patriarche, G. Shear-driven phase transformation in silicon nanowires. *Nanotechnology* **2018**, *29*, 125601.

(16) Galvão Tizei, L. H.; Amato, M. Electronic structure and optical properties of semiconductor nanowires polytypes. *Eur. Phys. J. B* **2020**, *93*, 16.

(17) Cartoixà, X.; Palummo, M.; Hauge, H. I. T.; Bakkers, E. P. A. M.; Rurali, R. Optical Emission in Hexagonal SiGe Nanowires. *Nano Lett.* **2017**, *17*, 4753–4758.

(18) Fadaly, E. M. T.; Dijkstra, A.; Suckert, J. R.; Ziss, D.; van Tilburg, M. A. J.; Mao, C.; Ren, Y.; van Lange, V. T.; Korzun, K.; Kölling, S. et al. Direct-bandgap emission from hexagonal Ge and SiGe alloys. *Nature* **2020**, *580*, 205–209.

(19) Zardo, I.; Yazji, S.; Hörmann, N.; Hertenberger, S.; Funk, S.; Mangialardo, S.; Morkötter, S.; Koblmüller, G.; Postorino, P.; Abstreiter, G. E1(A) Electronic Band Gap in Wurtzite InAs Nanowires Studied by Resonant Raman Scattering. *Nano Lett.* **2013**, *13*, 3011–3016.

(20) De Luca, M.; Polimeni, A. Electronic properties of wurtzite-phase InP nanowires determined by optical and magneto-optical spectroscopy. *Appl. Phys. Rev.* **2017**, *4*, 041102.

(21) Senichev, A.; Corfdir, P.; Brandt, O.; Ramsteiner, M.; Breuer, S.; Schilling, J.; Geelhaar, L.; Werner, P. Electronic properties of wurtzite GaAs: A correlated structural, optical, and theoretical analysis of the same polytypic GaAs nanowire. *Nano Res.* **2018**, *11*, 4708–4721.

(22) Spirkoska, D.; Arbiol, J.; Gustafsson, A.; Conesa-Boj, S.; Glas, F.; Zardo, I.; Heigoldt, M.; Gass, M. H.; Bleloch, A. L.; Estrade, S. et al. Structural and optical properties of high quality zinc-blende/wurtzite GaAs nanowire heterostructures. *Phys. Rev. B* **2009**, *80*, 245325.

(23) Heiss, M.; Conesa-Boj, S.; Ren, J.; Tseng, H.-H.; Gali, A.; Rudolph, A.; Uccelli, E.; Peiró, F.; Morante, J. R.; Schuh, D.; Reiger, E.; Kaxiras, E.; Arbiol, J.; Fontcuberta i Morral, A. Direct correlation of crystal structure and optical properties in wurtzite/zinc-blende GaAs nanowire heterostructures. *Phys. Rev. B* **2011**, *83*, 045303.

(24) De Luca, M.; Zilli, A.; Fonseka, H. A.; Mokkapati, S.; Miriametro, A.; Tan, H. H.; Smith, L. M.; Jagadish, C.; Capizzi, M.; Polimeni, A. Polarized Light Absorption in Wurtzite InP Nanowire Ensembles. *Nano Lett.* **2015**, *15*, 998–1005.

(25) Zilli, A.; De Luca, M.; Tedeschi, D.; Fonseka, H. A.; Miriametro, A.; Tan, H. H.; Jagadish, C.; Capizzi, M.; Polimeni, A. Temperature Dependence of Interband Transitions in Wurtzite InP Nanowires. *ACS Nano* **2015**, *9*, 4277–4287.

(26) Assali, S.; Greil, J.; Zardo, I.; Belabbes, A.; de Moor, M. W. A.; Koelling, S.; Koenraad, P. M.; Bechstedt, F.; Bakkers, E. P. A. M.; Haverkort, J. E. M. Optical study of the band structure of wurtzite GaP nanowires. *J. Appl. Phys.* **2016**, *120*, 044304.

(27) Zardo, I.; Conesa-Boj, S.; Peiro, F.; Morante, J. R.; Arbiol, J.; Uccelli, E.; Abstreiter, G.; Fontcuberta i Morral, A. Raman spectroscopy of wurtzite and zinc-blende GaAs nanowires: Polarization dependence, selection rules, and strain effects. *Phys. Rev. B* **2009**, *80*, 245324.

(28) Raya-Moreno, M.; Aramberri, H.; Seijas-Bellido, J. A.; Cartoixà, X.; Rurali, R. Thermal conductivity of hexagonal Si and hexagonal Si nanowires from first-principles. *Appl. Phys. Lett.* **2017**, *111*, 032107.

(29) Raya-Moreno, M.; Rurali, R.; Cartoixà, X. Thermal conductivity for III-V and II-VI semiconductor wurtzite and zinc-blende polytypes: The role of anharmonicity and phase space. *Phys. Rev. Materials* **2019**, *3*, 084607.

(30) Fasolato, C.; De Luca, M.; Djomani, D.; Vincent, L.; Renard, C.; Di Iorio, G.; Paillard, V.; Amato, M.; Rurali, R.; Zardo, I. Crystalline, Phononic, and Electronic Properties of Heterostructured Polytypic Ge Nanowires by Raman Spectroscopy. *Nano Lett.* **2018**, *18*, 7075–7084.

(31) de Matteis, D.; De Luca, M.; Fadaly, E. M. T.; Verheijen, M. A.; López-Suárez, M.; Rurali, R.; Bakkers, E. P. A. M.; Zardo, I. Probing Lattice Dynamics and Electronic Resonances in Hexagonal Ge abd Si_xGe_{1-x} Alloys in Nanowires by Raman Spectroscopy. *ACS Nano* **2020**, *14*, 6845–6856.

(32) Glas, F.; Harmand, J.-C.; Patriarche, G. Why Does Wurtzite Form in Nanowires of III-V Zinc Blende Semiconductors? *Phys. Rev. Lett.* **2007**, *99*, 146101.

(33) Dubrovskii, V. G.; Sibirev, N. V.; Harmand, J. C.; Glas, F. Growth kinetics and crystal structure of semiconductor nanowires. *Phys. Rev. B* **2008**, *78*, 235301.

(34) Dubrovskii, V. G.; Sibirev, N. V. Growth thermodynamics of nanowires and its application to polytypism of zinc blende III-V nanowires. *Phys. Rev. B* **2008**, *77*, 035414.

(35) Zheng, H.; Wang, J.; Huang, J. Y.; Wang, J.; Zhang, Z.; Mao, S. X. Dynamic Process of Phase Transition from Wurtzite to Zinc Blende Structure in InAs Nanowires. *Nano Lett.* **2013**, *13*, 6023–6027.

(36) Corfdir, P.; Van Hattem, B.; Uccelli, E.; Conesa-Boj, S.; Lefebvre, P.; Fontcuberta i Morral, A.; Phillips, R. T. Three-Dimensional Magneto-Photoluminescence as a Probe of the Electronic Properties of Crystal-Phase Quantum Disks in GaAs Nanowires. *Nano Lett.* **2013**, *13*, 5303–5310.

(37) Tedeschi, D.; Fonseka, H. A.; Blundo, E.; Granados del Águila, A.; Guo, Y.; Tan, H. H.; Christianen, P. C. M.; Jagadish, C.; Polimeni, A.; De Luca, M. Hole and Electron Effective Masses in Single InP Nanowires with a Wurtzite-Zincblende Homojunction. *ACS Nano* **2020**, *14*, 11613–11622.

(38) Caroff, P.; Dick, K. A.; Johansson, J.; Messing, M. E.; Deppert, K.; Samuelson, L. Controlled polytypic and twin-plane superlattices in III–V nanowires. *Nat. Nanotech.* **2009**, *4*, 50–55.

(39) Dick, K. A.; Thelander, C.; Samuelson, L.; Caroff, P. Crystal Phase Engineering in Single InAs Nanowires. *Nano Lett.* **2010**, *10*, 3494–3499.

(40) Algra, R. E.; Verheijen, M. A.; Borgström, M. T.; Feiner, L.-F.; Immink, G.; van Enckevort, W. J. P.; Vlieg, E.; Bakkers, E. P. A. M. Twinning superlattices in indium phosphide nanowires. *Nature* **2008**, *456*, 369–372.

(41) Burgess, T.; Breuer, S.; Caroff, P.; Wong-Leung, J.; Gao, Q.; Hoe Tan, H.; Jagadish, C. Twinning Superlattice Formation in GaAs Nanowires. *ACS Nano* **2013**, *7*, 8105–8114.

(42) Zhang, L.; Luo, J.-W.; Zunger, A.; Akopian, N.; Zwiller, V.; Harmand, J.-C. Wide InP Nanowires with Wurtzite/Zincblende Superlattice Segments Are Type-II whereas Narrower

Nanowires Become Type-I: An Atomistic Pseudopotential Calculation. *Nano Lett.* **2010**, *10*, 4055–4060.

(43) Amato, M.; Kaewmaraya, T.; Zobelli, A.; Palummo, M.; Rurali, R. Crystal Phase Effects in Si Nanowire Polytypes and Their Homojunctions. *Nano Lett.* **2016**, *16*, 5694–5700.

(44) De Luca, M.; Fasolato, C.; Verheijen, M. A.; Ren, Y.; Swinkels, M. Y.; Kölling, S.; Bakkers, E. P. A. M.; Rurali, R.; Cartoixà, X.; Zardo, I. Phonon Engineering in Twinning Superlattice Nanowires. *Nano Lett.* **2019**, *19*, 4702–4711.

(45) Carrete, J.; López-Suárez, M.; Raya-Moreno, M.; Bochkarev, A. S.; Royo, M.; Madsen, G. K. H.; Cartoixà, X.; Mingo, N.; Rurali, R. Phonon transport across crystal-phase interfaces and twin boundaries in semiconducting nanowires. *Nanoscale* **2019**, *11*, 16007–16016.

(46) Corfdir, P.; Lewis, R. B.; Marquardt, O.; Küpers, H.; Grandal, J.; Dimakis, E.; Trampert, A.; Geelhaar, L.; Brandt, O.; Phillips, R. T. Exciton recombination at crystal-phase quantum rings in GaAs/$In_xGa_{1-x}As$ core/multishell nanowires. *Appl. Phys. Lett.* **2016**, *109*, 082107.

(47) Royo, M.; Luca, M. D.; Rurali, R.; Zardo, I. A review on III-V core-multishell nanowires: growth, properties, and applications. *J. Phys. D: Appl. Phys.* **2017**, *50*, 143001.

(48) Kresse, G.; Furthmüller, J. Efficient iterative schemes for ab initio total-energy calculations using a plane-wave basis set. *Phys. Rev. B* **1996**, *54*, 11169.

(49) Blöchl, P. E. Projector augmented-wave method. *Phys. Rev. B* **1994**, *50*, 17953.

(50) Kresse, G.; Joubert, D. From ultrasoft pseudopotentials to the projector augmented-wave method. *Phys. Rev. B* **1999**, *59*, 1758.

(51) El-Mellouhi, F.; Mousseau, N.; Ordejón, P. Sampling the diffusion paths of a neutral vacancy in silicon with quantum mechanical calculations. *Phys. Rev. B* **2004**, *70*, 205202.

(52) Sholihun,; Ishii, F.; Saito, M. First-principles calculations of multivacancies in germanium. *Jpn. J. Appl. Phys.* **2015**, *55*, 011301.

(53) Amato, M.; Ossicini, S.; Canadell, E.; Rurali, R. Preferential Positioning, Stability, and Segregation of Dopants in Hexagonal Si Nanowires. *Nano Lett.* **2019**, *19*, 866–876.

(54) Amato, M.; Kaewmaraya, T.; Zobelli, A. Extrinsic Doping in Group IV Hexagonal-Diamond-Type Crystals. *J. Phys. Chem. C* **2020**, *124*, 17290–17298.

(55) Leslie, M.; Gillan, N. J. The energy and elastic dipole tensor of defects in ionic crystals calculated by the supercell method. *J. Phys. C: Solid State Phys.* **1985**, *18*, 973–982.

(56) Makov, G.; Payne, M. C. Periodic boundary conditions in ab initio calculations. *Phys. Rev. B* **1995**, *51*, 4014–4022.

(57) Freysoldt, C.; Neugebauer, J.; de Walle, C. G. V. Fully Ab Initio Finite-Size Corrections for Charged-Defect Supercell Calculations. *Phys. Rev. Lett.* **2009**, *102*, 016402.

(58) Freysoldt, C.; Neugebauer, J.; Van de Walle, C. G. Electrostatic interactions between charged defects in supercells. *phys. stat. sol. (b)* **2011**, *248*, 1067–1076.

(59) Freysoldt, C.; Grabowski, B.; Hickel, T.; Neugebauer, J.; Kresse, G.; Janotti, A.; Van de Walle, C. G. First-principles calculations for point defects in solids. *Rev. Mod. Phys.* **2014**, *86*, 253–305.

(60) Ziman, J. M. *Principles of the Theory of Solids*, 2nd ed.; 1972; pp 37–41.

(61) Ewald, P. P. Die Berechnung optischer und elektrostatischer Gitterpotentiale. *Annalen der Physik* **1921**, *369*, 253–287.

(62) Rurali, R.; Cartoixà, X. Theory of Defects in One-Dimensional Systems: Application to Al-Catalyzed Si Nanowires. *Nano Lett.* **2009**, *9*, 975–979.

(63) Rurali, R.; Palummo, M.; Cartoixà, X. Convergence study of neutral and charged defect formation energies in Si nanowires. *Phys. Rev. B* **2010**, *81*, 235304.

(64) Zhang, S. B.; Northrup, J. E. Chemical potential dependence of defect formation energies in GaAs: Application to Ga self-diffusion. *Phys. Rev. Lett.* **1991**, *67*, 2339–2342.

(65) Northrup, J. E.; Zhang, S. B. Dopant and defect energetics: Si in GaAs. *Phys. Rev. B* **1993**, *47*, 6791–6794.

(66) Van de Walle, C. G. Energies of various configurations of hydrogen in silicon. *Phys. Rev. B* **1994**, *49*, 4579–4585.

(67) Van de Walle, C. G.; Laks, D. B.; Neumark, G. F.; Pantelides, S. T. First-principles calculations of solubilities and doping limits: Li, Na, and N in ZnSe. *Phys. Rev. B* **1993**, *47*, 9425–9434.

(68) Luo, X.; Zhang, S. B.; Wei, S.-H. Theory of Mn supersaturation in Si and Ge. *Phys. Rev. B* **2004**, *70*, 033308.

(69) Fahey, P. M.; Griffin, P. B.; Plummer, J. D. Point defects and dopant diffusion in silicon. *Rev. Mod. Phys.* **1989**, *61*, 289–384.

(70) Stumpf, R.; Scheffler, M. Theory of self-diffusion at and growth of Al(111). *Phys. Rev. Lett.* **1994**, *72*, 254–257.

(71) Aradi, B.; Gali, A.; Deák, P.; Lowther, J. E.; Son, N. T.; Janzén, E.; Choyke, W. J. Ab initio density-functional supercell calculations of hydrogen defects in cubic SiC. *Phys. Rev. B* **2001**, *63*, 245202.

(72) Yeh, C.-Y.; Lu, Z. W.; Froyen, S.; Zunger, A. Zinc-blende–wurtzite polytypism in semiconductors. *Phys. Rev. B* **1992**, *46*, 10086–10097.

(73) Ito, T. Simple Criterion for Wurtzite-Zinc-Blende Polytypism in Semiconductors. *Jpn. J. Appl. Phys.* **1998**, *37*, L1217–L1220.

(74) García, A.; Cohen, M. L. First-principles ionicity scales. I. Charge asymmetry in the solid state. *Phys. Rev. B* **1993**, *47*, 4215–4220.

(75) García, A.; Cohen, M. L. First-principles ionicity scales. II. Structural coordinates from atomic calculations. *Phys. Rev. B* **1993**, *47*, 4221–4225.

(76) Abu-Farsakh, H.; Qteish, A. Ionicity scale based on the centers of maximally localized Wannier functions. *Phys. Rev. B* **2007**, *75*, 085201 .

(77) Wei, S.-H.; Zunger, A. Predicted band-gap pressure coefficients of all diamond and zinc-blende semiconductors: Chemical trends. *Phys. Rev. B* **1999**, *60*, 5404–5411.

(78) Yeh, C.-Y.; Wei, S.-H.; Zunger, A. Relationships between the band gaps of the zinc-blende and wurtzite modifications of semiconductors. *Phys. Rev. B* **1994**, *50*, 2715–2718.

(79) Lany, S.; Zunger, A. Assessment of correction methods for the band-gap problem and for finite-size effects in supercell defect calculations: Case studies for ZnO and GaAs. *Phys. Rev. B* **2008**, *78*, 235104.

(80) Giorgi, G.; Van Schilfgaarde, M.; Korkin, A.; Yamashita, K. On the Chemical Origin of the Gap Bowing in $(GaAs)_{1-x}Ge_{2x}$ Alloys: A Combined DFT-QSGW Study. *Nanoscale Res. Lett.* **2010**, *5*, 469–477.

(81) Ley, L.; Pollak, R. A.; McFeely, F. R.; Kowalczyk, S. P.; Shirley, D. A. Total valence-band densities of states of III-V and II-VI compounds from x-ray photoemission spectroscopy. *Phys. Rev. B* **1974**, *9*, 600–621.

(82) Lautenschlager, P.; Garriga, M.; Logothetidis, S.; Cardona, M. Interband critical points of GaAs and their temperature dependence. *Phys. Rev. B* **1987**, *35*, 9174–9189.

(83) Zanolli, Z.; Fuchs, F.; Furthmüller, J.; von Barth, U.; Bechstedt, F. Model GW band structure of InAs and GaAs in the wurtzite phase. *Phys. Rev. B* **2007**, *75*, 245121.

(84) Zanolli, Z. private communication.

(85) Tedeschi, D.; De Luca, M.; Granados del Aguila, A.; Gao, Q.; Ambrosio, G.; Capizzi, M.; Tan, H. H.; Christianen, P.; Jagadish, C.; Polimeni, A. Value and anisotropy of the electron and hole mass in pure wurtzite InP nanowires. *Nano Lett.* **2016**, *16*, 6213–6221.

(86) Mishra, A.; Titova, L. V.; Hoang, T. B.; Jackson, H. E.; Smith, L. M.; Yarrison-Rice, J. M.; Kim, Y.; Joyce, H. J.; Gao, Q.; Tan, H. H.; Jagadish, C. Polarization and temperature dependence of photoluminescence from zincblende and wurtzite InP nanowires. *Appl. Phys. Lett.* **2007**, *91*, 263104.

(87) Belabbes, A.; Panse, C.; Furthmüller, J.; Bechstedt, F. Electronic bands of III-V semiconductor polytypes and their alignment. *Phys. Rev. B* **2012**, *86*, 075208.

(88) Belabbes, A.; Bechstedt, F. Forbidden Band-Edge Excitons of Wurtzite-GaP: A Theoretical View. *phys. stat. sol. (b)* **2019**, *256*, 1800238.

(89) Giorgi, G.; Yamashita, K. Amphoteric behavior of Ge in GaAs: an LDA analysis. *Model. Simul. Mater. Sci. Eng.* **2011**, *19*, 035001.

(90) Galicka, M.; Buczko, R.; Kacman, P. Segregation of Impurities in GaAs and InAs Nanowires. *J. Phys. Chem. C* **2013**, *117*, 20361–20370.

(91) Diao, Y.; Liu, L.; Xia, S. Exploration the p-type doping mechanism of GaAs nanowires from first-principles study. *Phys. Lett. A* **2019**, *383*, 202–209.

(92) Du, Y. A.; Sakong, S.; Kratzer, P. As vacancies, Ga antisites, and Au impurities in zinc blende and wurtzite GaAs nanowire segments from first principles. *Phys. Rev. B* **2013**, *87*, 075308 .

(93) Coutinho, J.; Torres, V. J. B.; Jones, R.; Briddon, P. R. Electrical activity of chalcogen-hydrogen defects in silicon. *Phys. Rev. B* **2003**, *67*, 035205.

(94) Alkauskas, A.; Broqvist, P.; Pasquarello, A. Defect Energy Levels in Density Functional Calculations: Alignment and Band Gap Problem. *Phys. Rev. Lett.* **2008**, *101*, 046405.

(95) Komsa, H.-P.; Broqvist, P.; Pasquarello, A. Alignment of defect levels and band edges through hybrid functionals: Effect of screening in the exchange term. *Phys. Rev. B* **2010**, *81*, 205118.

(96) Alkauskas, A.; Pasquarello, A. Band-edge problem in the theoretical determination of defect energy levels: The O vacancy in ZnO as a benchmark case. *Phys. Rev. B* **2011**, *84*, 125206.

(97) Graham, A. M.; Corfdir, P.; Heiss, M.; Conesa-Boj, S.; Uccelli, E.; Fontcuberta i Morral, A.; Phillips, R. T. Exciton localization mechanisms in wurtzite/zinc-blende GaAs nanowires. *Phys. Rev. B* **2013**, *87*, 125304.

(98) De Luca, M.; Rubini, S.; Felici, M.; Meaney, A.; Christianen, P. C. M.; Martelli, F.; Polimeni, A. Addressing the Fundamental Electronic Properties of Wurtzite GaAs Nanowires by High-Field Magneto-Photoluminescence Spectroscopy. *Nano Lett.* **2017**, *17*, 6540–6547.

Table 1: Lattice parameters, relative dielectric constants, and G_0W_0 bandgaps (LDA values are indicated in parenthesis).

		a (Å)	c (Å)	ε_{xx}	ε_{zz}	Bandgap (eV)
GaAs	zincblende	5.601	-	13.75	13.75	1.66 (0.54)
	wurtzite	3.946	6.510	12.80	13.03	1.46 (0.55)
GaP	zincblende	5.381	-	10.52	10.52	2.17 (1.39)
	wurtzite	3.790	6.254	10.16	10.60	2.28 (1.32)
InP	zincblende	5.821	-	11.41	11.41	1.42 (0.62)
	wurtzite	4.107	6.748	10.73	10.96	1.49 (0.68)

Table 2: Difference in the neutral and charged impurity formation energy, ΔE_{form}, between the ZB and the WZ structures (a positive value indicates that the WZ is more stable) for the series of acceptor impurities studied. All energies are given in meV/f.u. We also report the difference in transition energies, $\Delta E(0/-)$, between the ZB and the WZ structures (a positive value indicates that the impurity state in WZ is shallower).

	GaAs			GaP	InP
	Si_{As}	C_{As}	Zn_{Ga}	Zn_{P}	Zn_{P}
$\Delta E^{0}_{\mathrm{form}}$	187	248	197	94	33
$\Delta E^{-1}_{\mathrm{form}}$	201	265	210	119	39
$\Delta E(0/-)$	14	17	13	25	6

Table 3: Difference in the neutral and charged impurity formation energy, ΔE_{form}, between the ZB and the WZ structures (a positive value indicates that the WZ is more stable) for the series of donor impurities studied. All energies are given in meV/f.u. We also report the difference in transition energies, $\Delta E(+/0)$, between the ZB and the WZ structures (a positive value indicates that the impurity state in ZB is shallower).

	GaAs	GaP		InP
	Si_{Ga}	S_P	Te_P	Te_P
$\Delta E^{0}_{\mathrm{form}}$	152	-7	-39	20
$\Delta E^{+1}_{\mathrm{form}}$	-8	-130	-122	-117
$\Delta E(+/0)$	160	123	83	137

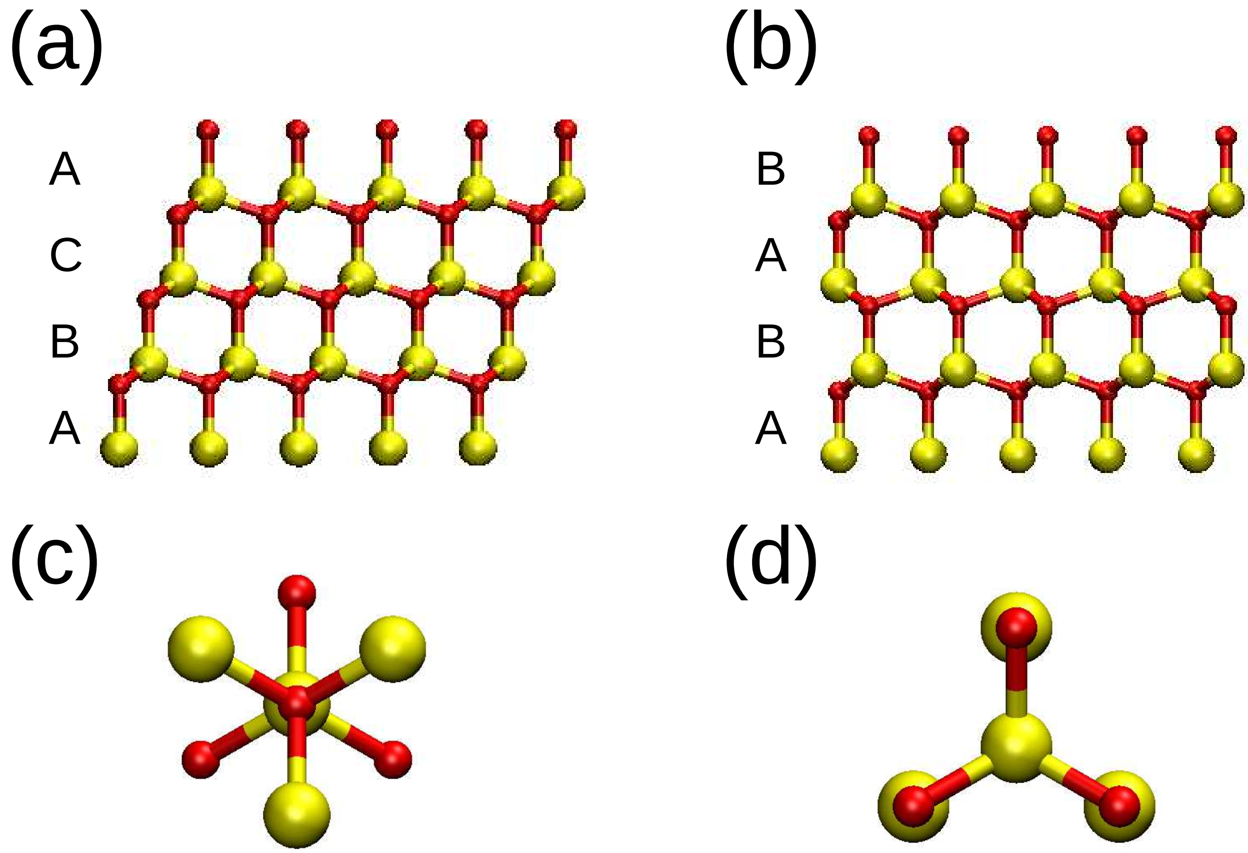

Figure 1: Side view of (a) the ZB and (b) the WZ lattice structure where the ABCABC vs ABABAB stacking along the cubic [111] axis can be appreciated. (c) Staggered and (d) eclipsed dihedral conformation of the ZB and WZ crystal phases.

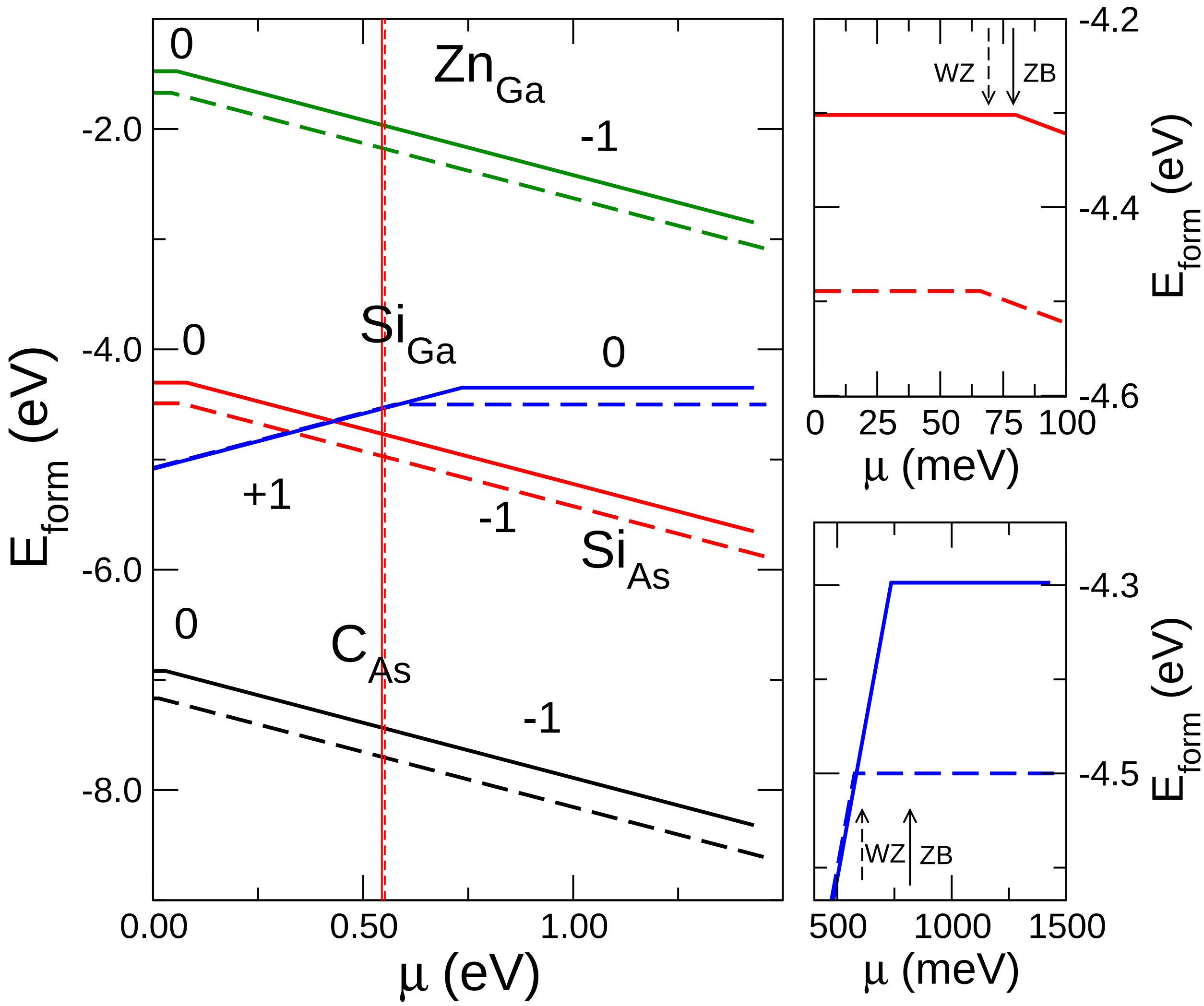

Figure 2: Formation energies as a function of the chemical potential of the electron of Si, C, and Zn in ZB (continuous line) and WZ (dashed line) GaAs. The side panels show zoomed views of Si_{As} (top) and Si_{Ga} (bottom).

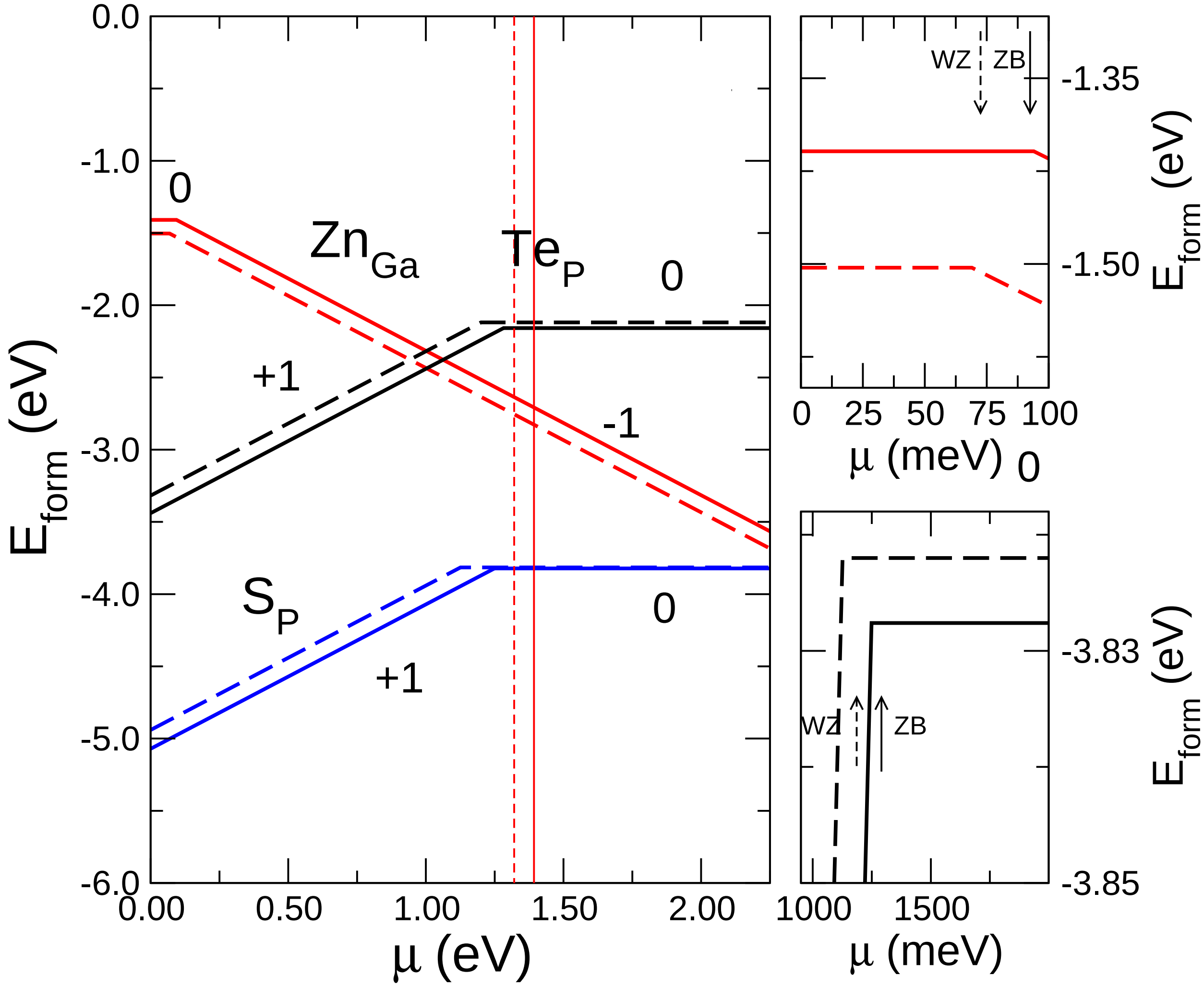

Figure 3: Formation energies as a function of the chemical potential of the electron of Te, S, and Zn in ZB (continuous line) and WZ (dashed line) GaP. The side panels show zoomed views of Zn_{Ga} (top) and Te_P (bottom).

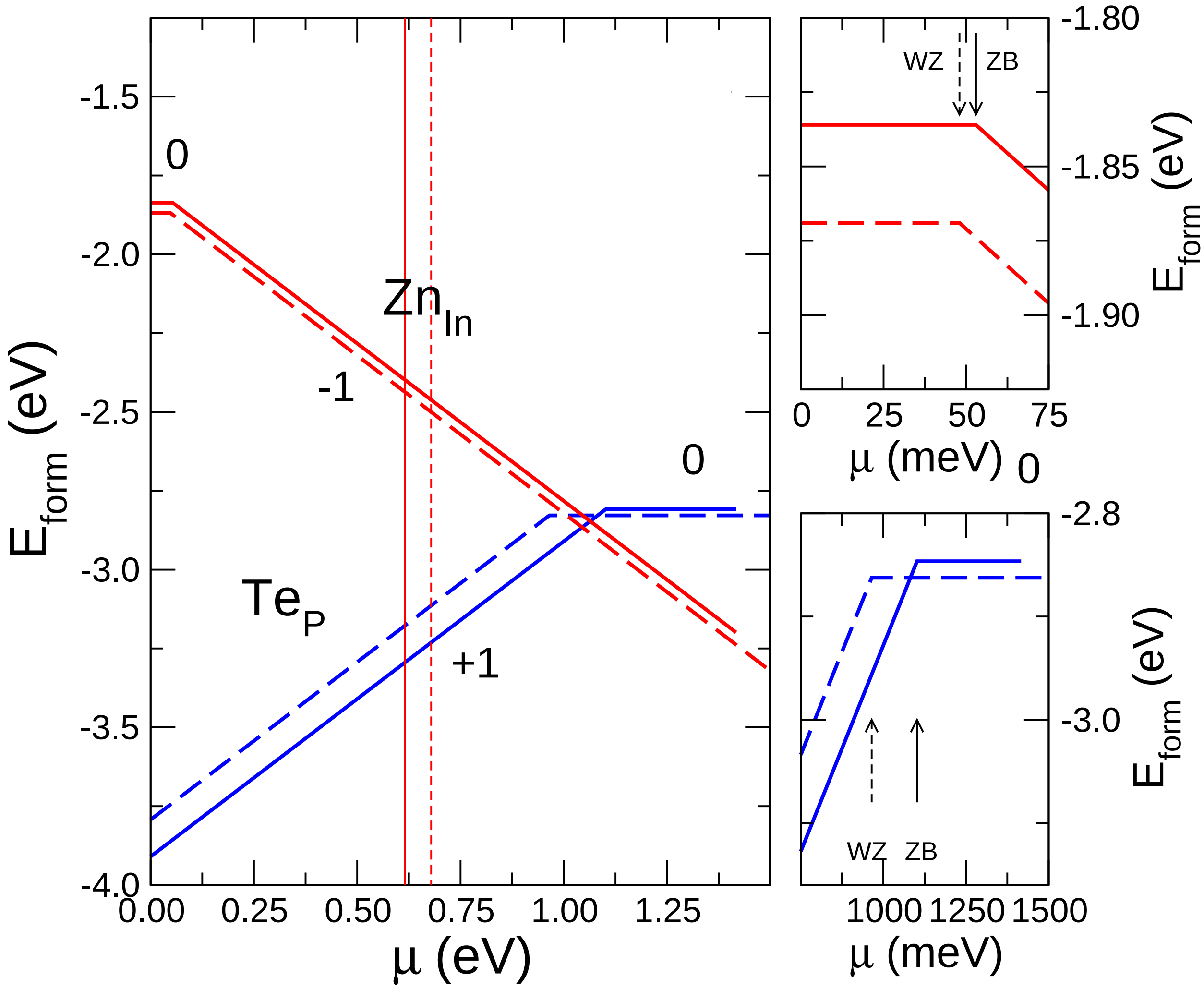

Figure 4: Formation energies as a function of the chemical potential of the electron of Te and Zn in ZB (continuous line) and WZ (dashed line) InP. The side panels show zoomed views of Zn_{In} (top) and Te_P (bottom).